AIAA SciTech Forum
7-11 January 2019, San Diego, California
AIAA Scitech 2019 Forum

10.2514/6.2019-2169

Low-Mach-Number Simulation of Diffusion Flames with the Chemical-Diffusive Model

Joseph D. Chung*, Xiao Zhang*, Carolyn R. Kaplan†, and Elaine S. Oran‡
University of Maryland, College Park, MD, 20742

This work describes and tests the calibration process of the chemical-diffusive model (CDM) for the simulation of non-premixed diffusion flames. The CDM is an alternative, simplified approach for incorporating the effects of combustion in a fluid simulation, based on the ideas of regulating the rate of energy release such that the properties of combustion waves (e.g. flames and detonations) are reproduced. Past implementations of the CDM have considered single-stoichiometry fuel-air mixtures or mixtures with variable stoichiometry but with premixed modes of combustion. In this work, the CDM is tested and shown to work for non-premixed, low-Mach-number flames (i.e., diffusion flames) by incorporating it into a numerical model which solves the reactive and compressible Navier-Stokes equations with the barely implicit correction (BIC) algorithm, which removes the acoustic limit on the integration time-step size. Simulations of one-dimensional premixed laminar flames reproduce the required premixed laminar flame speed, thickness, and temperature. A two-dimensional, steady-state, laminar coflow diffusion flame is computed, and the result demonstrates the ability of the algorithm to compute a non-premixed flame. Lastly, a two-dimensional simulation of two opposing jets of fuel and air show that the CDM approach can compute the structure of a counter-flow diffusion flame.

I. Introduction

Reactive-flow simulations have benefited significantly from the progress made in algorithms and methodologies that solve the governing fluid equations and chemical reactions. There is a large body of ongoing research that addresses these areas, including the difficulty of coupling fluid dynamics and combustion models. A significant portion of this difficulty arises from the orders-of-magnitude variation in temporal and spatial scales within and between the combustion and fluid processes.

The combustion process is often modeled using detailed and skeletal chemical mechanisms, which are important for resolving effects due to chemical kinetics but generally require including many chemical species and reactions. These species and reactions can have large variations in transport properties and reaction rates within a single mechanism, introducing stiffness to the time-step integration. Furthermore, resolving the transport of n species requires solving n equations, in addition to the conservation laws of mass, momentum, and energy. These challenges can make reactive flow computations which use detailed mechanisms prohibitively expensive, even at small scales.

To reduce the numerical cost, a simplified combustion model can be an attractive alternative. This is especially true when the effects of heat release are the primary interest rather than the details of the chemical kinetics. The rate of heat release, in the simplest form, can be regulated by the conversion rate (i.e., the reaction rate) of reactants to products. A one-step, irreversible reaction can be used to represent this conversion, which might be governed by a rate that has an Arrhenius form,

$$\dot{\omega} = A \exp(-E_a/R_u T) C_f^a C_o^b \tag{1}$$

where $\dot{\omega}$ is the reaction rate, E_a is the activation energy, R_u is the universal gas constant, T is the temperature, C_f and C_o are the concentrations of fuel and oxidizer, respectively, and a and b are the reaction

*Graduate Research Assistant, Dept. of Aerospace Engineering, 3202 James M. Patterson Bldg., and AIAA Student Member.
†Research Associate Professor, Dept. of Aerospace Engineering, 3202 James M. Patterson Bldg., and AIAA Associate Fellow
‡Glenn L. Martin Institute Professor of Engineering, Dept. of Aerospace Engineering, 3232 Jeong H. Kim Engineering Bldg., and AIAA Honorary Fellow.

orders. The heat release rate is then given by $q\omega$, where q is the heat of reaction. This approach was shown to work well for matching low-speed combustion wave properties of a mixture. One early example is by Westbrook and Dryer [1], who investigated the use of such a simplified single-step mechanism to model the slow burning of hydrocarbons and oxygen. They showed that one could match laminar flame speeds and flame temperatures from premixed experiments by calibrating and optimizing the parameters used in Eq. 1. Fernandez-Tarrazo et al. [2] demonstrated the capability of the single-step model to predict the structure of non-premixed, diffusion flames, along with the correct flame temperatures and speeds of hydrocarbon-air premixed mixtures, by allowing for the heat of reaction and activation energy to vary according to the equivalence ratio.

Although these examples are for diffusion-limited combustion waves, simplified mechanisms have also been successful for matching detonation properties. The first such method is the induction parameter model (IPM) [3] by Oran et al., which allowed heat release in a control volume based on the local state of the reaction and thermodynamic variables. Though succesfully used for modeling detonations, the formulation of the IPM does make sense for computing flames.

Following the IPM, there has been a body of work (we list a selected few: [4, 5, 6, 7]) which developed and used a simplified combustion model that could be used for both flames and detonations. This model was called the chemical-diffusive model (CDM), which also uses the functional form of a single-step Arrhenius rate to regulate the heat release. The CDM is based on a calibration of the parameters for the Arrhenius rate, along with the heat of combustion and heat diffusivity, such that the properties of *both* the subsonic flame and supersonic detonation are reproduced in a reactive flow computation. These properties have traditionally been the premixed flame speed, flame thickness, detonation speed, detonation half-reaction thickness, and the adiabatic constant-pressure and constant-volume temperatures. The CDM has been applied to the simulation of deflagration-to-detonation transitions (DDT) for mixtures with single and, more recently, variable stoichiometry [8, 9]. The principles behind the calibration of the CDM are discussed further in [7, 8] and recently, an automated procedure for this calibration process was introduced in [9].

Prior applications of the CDM, however, focused on premixed modes of combustion, where combustion waves are limited by the amount of compression from a shock wave or by the diffusion of heat from products to reactants. In this work, we apply a simplified CDM calibration procedure, which considers only premixed flames and forgoes matching the detonation properties. We repeat this procedure for varying values of the stoichiometry and then apply the calibrated CDM to computations of non-premixed diffusion flames.

In the following section, we describe the model, the calibration process, and present the model parameters for a mixture of n-Heptane and air as a function of equivalence ratio. In section III, we briefly describe and outline the fluid algorithm used to solve the reactive Navier-Stokes equations. Section IV presents three test cases for this combined fluid-combustion algorithm: a 1D laminar premixed flame, 2D laminar coflow diffusion flame, and a 2D counter-flow diffusion flame.

II. Calibration of the Chemical-Diffusive Model for Flames

The objective of the CDM is to capture specific burning properties of a fuel-oxidizer mixture in a Navier-Stokes computation, and without the cost entailed by detailed chemical mechanisms. This is done by using the simplest formulation of an irreversible chemical reaction,

$$Reactants \longrightarrow Products. \tag{2}$$

This formulation is used regardless of stoichiometry, which means that for rich or lean mixtures, the remaining reactants after complete burning are implicitly grouped with the products. The rate of conversion from reactants to products is governed by an Arrhenius-type rate,

$$\Omega = A\rho Y \exp(-E_a/R_u T), \tag{3}$$

where ρ is the fluid density, and Y is a reaction progress variable, which scales from 1 at the start of the reaction to 0 when the products are fully formed. The heat release rate is then given as

$$\dot{q} = q\Omega. \tag{4}$$

The CDM computes the diffusive processes using Fickian mass diffusion and Fourier heat conduction. The mass and heat diffusivities are modeled to have a temperature and density dependence,

$$D = D_0 \frac{T^n}{\rho}, \quad \kappa = \kappa_0 \frac{T^n}{\rho}, \tag{5}$$

where D and κ are the mass and heat diffusivities, respectively. The subscript 0 refers to a reference state with temperature T_0 and pressure P_0. The exponent n is chosen to be 0.7 and a unity Lewis number approximation is used, allowing us to set $D = \kappa$, consistent with prior applications of the CDM [4, 5, 10, 7].

The choice of CDM parameter values is critical to compute the correct burning properties of a reactive mixture. As discussed earlier, our calibration considers only laminar premixed flames. We will later show that this approach works reasonably well when used in computations of non-premixed diffusion flames.

For the chemical-parameter calibration, we choose to match three important properties: the constant-pressure adiabatic flame temperature T_b, the premixed laminar flame speed S_L, and thickness Δx_L. Together, these properties provide energy, length, and time-scale constraints. With three target combustion properties to match, we require three parameters to tune. For this, we look to the set of reaction Eqs. 3 and 4, from which q is used to match T_b, and subsequently a combination of A and E_a are used to match both S_L and Δx_L.

II.A. Determining q

The heat release q represents the total change in enthalpy from the unburned state to the burned state for a constant pressure, adiabatic, exothermic reaction. To determine its value, we first apply the approximation of a calorically perfect gas and a constant molecular weight M across all species. With these approximations, we can then express q as

$$q = (T_b - T_0)C_p \tag{6}$$

where C_p is the specific heat capacity at constant pressure. The reference temperature T_0 is generally set to be 300 K. For n-Heptane-air mixtures, we use the n-Heptane boiling temperature of 372 K at 1 atm. The values of T_b can be found from either empirical data or by using chemical equilibrium software and detailed reaction mechanisms. To account for varying equivalence ratio ϕ, q is computed for T_b corresponding to a particular value of ϕ such that

$$q(\phi) = (T_b(\phi) - T_0)C_p, \tag{7}$$

where $q(\phi)$ and $T_b(\phi)$ denote functions of ϕ.

II.B. Determining E_a and A

To compute E_a and A, we integrate an inviscid, one-dimensional, steady-state balance of heat conduction with convection and chemical heat release, assuming unity Lewis number,

$$\frac{d}{dx}\left(K\frac{dT}{dx}\right) = \rho\left(U_l C_p \frac{dT}{dx} - q\Omega\right). \tag{8}$$

Here, x is the spatial coordinate in the reference frame of the reaction wave, U_l is the fluid velocity, and K is the thermal conductivity given by

$$K = \kappa\rho C_p. \tag{9}$$

The values of κ are determined by Eq. 5, for which κ_0 is found from averaged values of detailed transport data. Details on the procedure to solve Eq. 8 are described in [7].

Equation 8 is a simplified energy balance across a premixed, laminar flame and allows for computing the temperature and velocity profile. These profiles are used to determine the flame thickness and flame speed. The flame speed S_L is given by U_l at the reactant inflow location $x = 0$. The flame thickness is computed according to

$$\Delta x_L = \frac{T_b - T_0}{\max|dT/dx|}. \tag{10}$$

The heat release rate $q\Omega$ in Eq. 8 is controlled by the parameters E_a and A. To determine their optimal values, they are iteratively varied until the computed flame thickness Δx_L and flame speed S_L of Eq. 8

match the values obtained from empirical data or detailed chemistry. Many root-finding algorithms will be able to perform this optimization. In this work, we use the Nelder-Mead algorithm.

Similar to determining $q(\phi)$, we account for varying stoichiometry by first determining $\Delta x_L(\phi)$ and $S_L(\phi)$ for a particular equivalence ratio ϕ. Then, the optimization process is repeated across an array of equivalence ratios, generating a corresponding array of E_a and A as a function of ϕ.

II.C. Optimized values of q, E_a, and A for n-Heptane-air

The target combustion properties are obtained using the Cantera python library [11] as the chemical equilibrium software and the 188-species skeletal n-Heptane mechanism [12]. The resulting flame temperature, speed, and thickness are shown in Fig. 1 as a function of equivalence ratio.

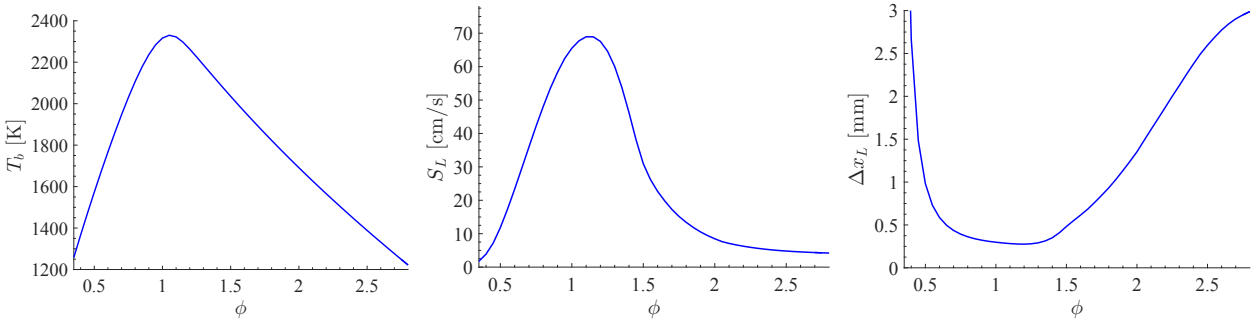

(a) Flame temperature T_b versus varying equivalence ratio.

(b) Flame speed S_L versus varying equivalence ratio.

(c) Flame thickness Δx_L versus varying equivalence ratio.

Figure 1. Target combustion properties computed from Cantera [11] with the 188-species skeletal n-Heptane mechanism [12].

After obtaining the target combustion properties, we apply the above procedure for an n-Heptane-air mixture, using a constant $M = 30.6\,\mathrm{g/mol}$ and specific heat ratio $\gamma = 1.18$ for all species and temperatures. The values of the normalized heat release, pre-exponential factor, and normalized activation energy are shown in Fig. 2 as a function of equivalence ratio. These values are tabulated as functions of the unburned, reactant equivalence ratio and accessed by a Navier-Stokes computation as a lookup table.

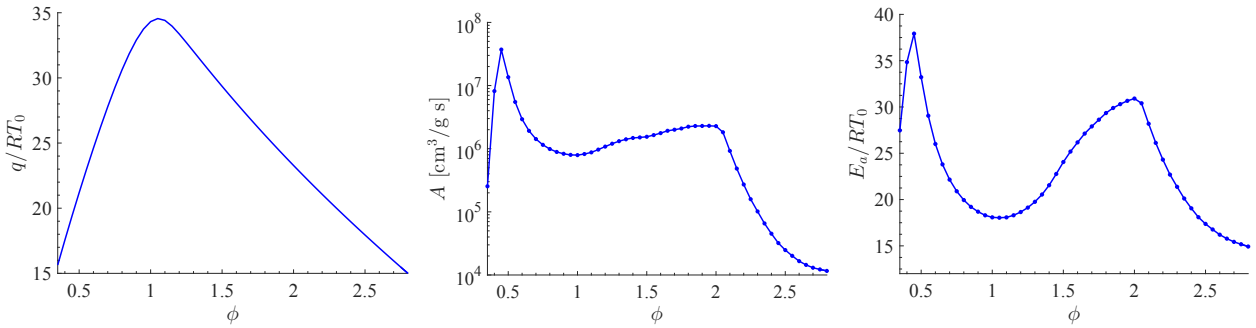

(a) Normalized heat release versus equivalence ratio.

(b) Pre-exponential factor versus equivalence ratio.

(c) Normalized activation energy versus equivalence ratio.

Figure 2. Optimized CDM parameters for ϕ in the range of 0.35 to 2.80 for heptane-air with $T_0 = 372\,\mathrm{K}$. E_a and A are incremented by 0.05 in equivalence ratio (shown as filled circles).

The procedure was also applied to methane-air, using $M = 27\,\mathrm{g/mol}$, $\gamma = 1.25$, and $T_0 = 300\,\mathrm{K}$. The target combustion properties were obtained using the GRI-Mech 3.0 mechanism [13]. The calibrated parameters will be presented in future work.

III. Reactive Navier-Stokes Algorithm

This work uses the CDM in a numerical model that solves the reactive Navier-Stokes (NS) equations,

$$\frac{\partial \rho}{\partial t} = -\nabla \cdot (\rho \mathbf{V}) \tag{11}$$

$$\frac{\partial (\rho \mathbf{V})}{\partial t} = -\nabla \cdot (\rho \mathbf{V}\mathbf{V}) - \nabla P - \nabla \cdot \hat{\tau} \tag{12}$$

$$\frac{\partial E}{\partial t} = -\nabla \cdot ((E + P)\,\mathbf{V}) - \nabla \cdot (\mathbf{V} \cdot \hat{\tau}) - \nabla \cdot (K \nabla T) + \dot{q} \tag{13}$$

$$\frac{\partial \rho Y_i}{\partial t} = -\nabla \cdot (\rho Y_i \mathbf{V}) + \nabla \cdot (\rho D \nabla Y_i) + \dot{\omega}_i \tag{14}$$

$$\hat{\tau} = \rho\nu \left(\frac{2}{3} (\nabla \cdot \mathbf{V})\,\mathbf{I} - (\nabla \mathbf{V}) - (\nabla \mathbf{V})^{\dagger} \right) \tag{15}$$

where t is time, P is pressure, E is total energy, $\mathbf{V}$ is the velocity vector, and I is the identity matrix. The mass fraction for each species is represented by Y_i, where the subscript i indicates the species. The species production rate is represented by $\dot{\omega}_i$, which is related to Ω by the stoichiometric burning rates of the reactant species. In this work, we consider three species: fuel, oxidizer, and product. All species share the same molecular weight and specific heat ratio. In Eq. (15) $\hat{\tau}$ is the stress tensor for a Newtonian fluid, with ν as the kinematic viscosity. We compute the specific internal energy by considering a perfect, ideal gas,

$$e = \frac{P}{\rho(\gamma - 1)}. \tag{16}$$

The equation of state used here is the ideal gas law,

$$P = \rho R T \tag{17}$$

where R is the specific gas constant. The total energy E can then be computed by summing the internal and kinetic energy,

$$E = \rho e + \frac{1}{2} \rho \mathbf{V^2}. \tag{18}$$

The heat release rate $\dot{q}$ in Eq. 13 is computed in the same way as Eq. 4. The reaction rate Ω in Eq. 4 is computed as a function of the local "unburned" equivalence ratio ϕ_u, a parameter that is analogous to the mixture fraction. The variable ϕ_u is found by computing the amount of fuel and oxidizer that was required to form the product material in a computational cell. This amount of fuel and oxidizer is then added to the fuel and oxidizer that has not been burned. This gives the unburned values of fuel and oxidizer mass fractions, which are used to compute ϕ_u. All CDM reaction parameters and diffusion coefficients are indexed in a lookup table according to ϕ_u.

We use the barely implicit correction (BIC) algorithm ([14, 15]) to remove the acoustic limit on the CFL time-step constraint, thereby avoiding the numerical expense of explicitly integrating the NS equations in a low-Mach-number flow. The use of this algorithm requires a time-splitting integration procedure. In this procedure, the first step is to compute the global time step using the convective CFL condition. Each of the diffusive processes, which include Fickian mass diffusion, Fourier heat conduction, and Newtonian viscosity, has its own explicit time-step limit due to numerical stability. We then compute these limits, including the limit for the reaction rate. The maximum reaction time-step is computed to be the amount of time required for a stoichiometric premixed flame to propagate across 10% of a computational cell. This can be expressed as

$$\Delta t_{chem} = \frac{\Delta x}{10 \cdot S_L(\phi = 1)} \tag{19}$$

where Δx is the width of a computational cell. If any of these non-convective processes require a smaller time step than the convective time step, we then integrate the chemistry and diffusion independent of the convection, using the smaller time step. This is often referred to as subcycling. The subcycling integration is performed until the subcycling time reaches the global convective time step.

In reality, reaction and transport processes occur simultaneously within the flame. Transport can pull reactants away from the reaction zone, causing incomplete burning, a lower flame temperature, and also flame extinction when the transport is not sufficiently balanced by the reaction. To reproduce this effect within a computation, we perform the subcycling by first explicitly integrating the diffusion processes for one subcycle time step, using the minimum time step requirement discussed earlier. We then integrate the chemistry for the same subcycle time-step. This staggered integration is repeated until the total subcycling integration time has reached the global convective time-step. All computations presented in this article use a convective CFL of 0.3.

After the subcycling, we compute the convective fluxes and apply the BIC pressure correction to the momentum and energy equations. Further details on the BIC time integration (without chemistry)and pressure correction can be found in [15]. The inclusion of chemical reactions will be described in future work.

The convective, hyperbolic fluxes are computed using an unsplit version of the fourth-order Boris and Book [16] implementation of flux-corrected transport (FCT). Flux limiting is performed using the Zalesak [17] multidimensional limiter with the monotone correction by DeVore [18]. All parabolic fluxes are spatially discretized using a second-order, three-point central scheme and integrated by first-order Euler explicit time-marching. The entire algorithm is incorporated into the BoxLib [19] adaptive mesh refinement framework for parallelization and grid refinement. All computations presented in this work, however, employ a uniform mesh.

IV. Test Problems

We apply the CDM with the BIC-FCT algorithm to three different test problems, each testing a different characteristic of laminar, low-speed, steady flames. We first simulate a series of one-dimensional, premixed, laminar flames to determine whether the calibrated parameters can reproduce the target combustion properties discussed earlier. Then, we compute a two-dimensional, coflow diffusion flame to asses the capability of the CDM to compute a non-premixed flame. Lastly, a simulation of a two-dimensional, counter-flow diffusion flame are presented.

IV.A. 1D Premixed Laminar Flames

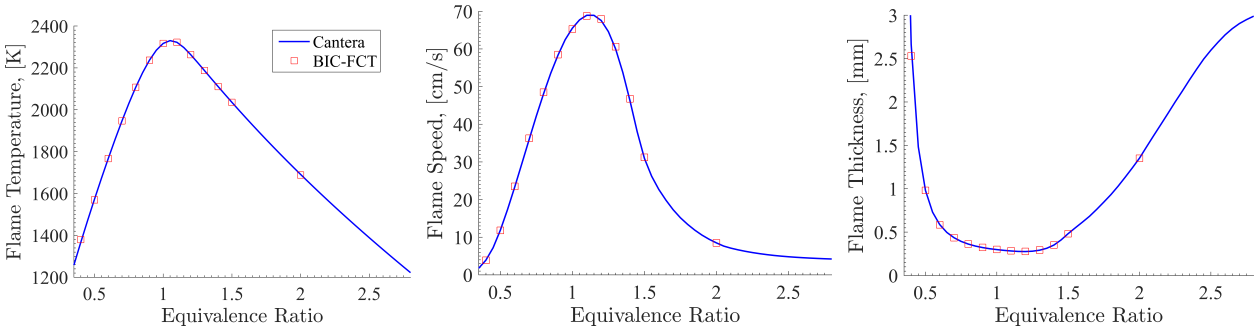

(a) Flame temperature T_b versus varying equivalence ratio.

(b) Flame speed S_L versus varying equivalence ratio.

(c) Flame thickness Δx_L versus varying equivalence ratio.

Figure 3. Blue lines are computed from Cantera [11] with the 188-species n-Heptane Lu and Law[12] mechanism. Red squares are computed using BIC-FCT-CDM.

The computational domain consists of an inflow and outflow boundary. The inflow specifies a temperature and also a velocity such that the flame remains within the computational domain. The outflow specifies a fixed pressure of 1 atm. All other primitive variables on both boundaries are extrapolated using a zero-gradient Neumann condition. For these computations, we use the parameters specified in Fig. 2 for n-Heptane-air mixtures. The inflow temperature is 372 K, consistent with the choice of T_0 in Section II. The flame thickness is computed using the simulated temperature profile of BIC-FCT-CDM and Eq. 10. Each case is computed with a specified inflow equivalence ratio. The equivalence ratio is varied from 0.35 to 2.0, and the steady-state results are shown in Fig. 3 as red squares, plotted with the target parameters (blue line) generated from Cantera and the 188-species skeletal mechanism. A uniform mesh is used, and for each equivalence

ratio, we maintain at least 16 cells within the flame thickness.

As seen in Fig. 3, there is strong agreement in all three properties of flame temperature, speed, and thickness with the 188-species mechanism. Thus the CDM, with the new calibrated parameters, can reproduce the target combustion properties. This result is also consistent with prior work using the CDM [7, 9].

Premixed laminar flames are also computed for methane-air mixtures with the same boundary conditions and configuration, except the inflow temperature which is set to be 300 K. Here, there is also strong agreement between the CDM and the GRI-Mech 3.0 mechanism. The results will be presented in a future work.

IV.B. 2D Coflow Diffusion Flame

We now assess whether the calibration approach taken in Section II can indeed compute a non-premixed flame by simulating a two-dimensional, coflow diffusion flame. The boundary conditions and domain size are shown in Fig. 4a. Here, the inflow boundary on the left has n-Heptane injected in the center with a constant temperature of 371.57 K and velocity of 5.67 cm/s. The inflow also has a parallel coflow of air with a temperature of 300 K and a faster velocity of 10.48 cm/s. The outflow boundary on the right is set to be a constant pressure of 1 atm, and the upper and lower walls are adiabatic symmetry planes. All other primitive variables at the inflow and outflow boundaries are extrapolated using a zero-gradient Neumann condition. The domain is discretized using a uniform, Cartesian mesh with $\Delta x = 28.4/2056$ cm.

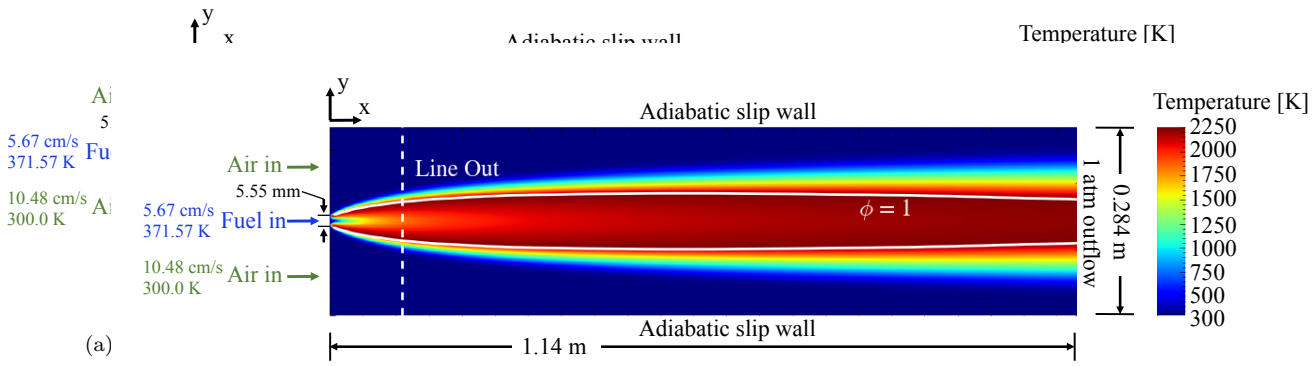

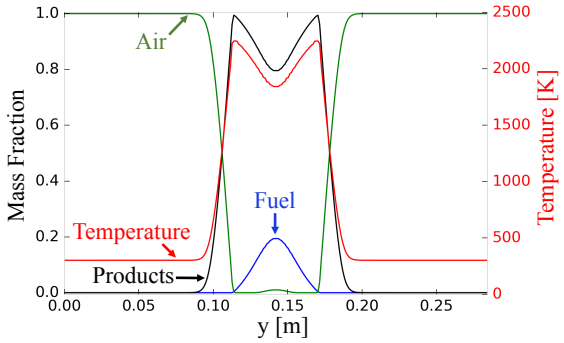

(b) The mass fractions of air, fuel, and product along with temperature along a line in the y direction as indicated by the dashed vertical white line in (a) of this figure.

Figure 4. A steady state computation of a 2D, laminar, n-Heptane and air, coflow diffusion flame.

Figure 4a also shows the steady-state temperature contour with a solid white line corresponding to the stoichiometric mixture fraction, i.e. the flame sheet. In Fig. 4b, we show the temperature, air, fuel, and product mass fractions along the vertical dashed white line in Fig. 4a. The peak temperature and maximum product concentration are located where the fuel and air are mostly depleted, as expected for a diffusion flame. In Fig. 4a, the peak temperature occurs near the flame sheet throughout the entire flow-field, also as expected. Also, the peak temperature does not exceed the maximum adiabatic flame temperature, indicating the balance of heat conduction and heat release rate for this non-premixed flame performs qualitatively well. These results suggest that the CDM approach to combustion can at least model the qualitative features of

a non-premixed flame.

IV.C. Two-Dimensional Counter-flow Diffusion Flame

Counter-flow diffusion flames are a canonical configuration for studying the structure and characteristics of non-premixed flames. Here, the flame sits between two opposed jets of oxidizer and fuel. This is different from the laminar coflow flame in that species diffusion occurs parallel to the bulk flow velocity. In the laminar coflow configuration, species diffusion is generally perpendicular to the bulk flow velocity. Therefore, the effect of transport on the flame is different; the result is that the strain effect is more dominant in the counter-flow configuration.

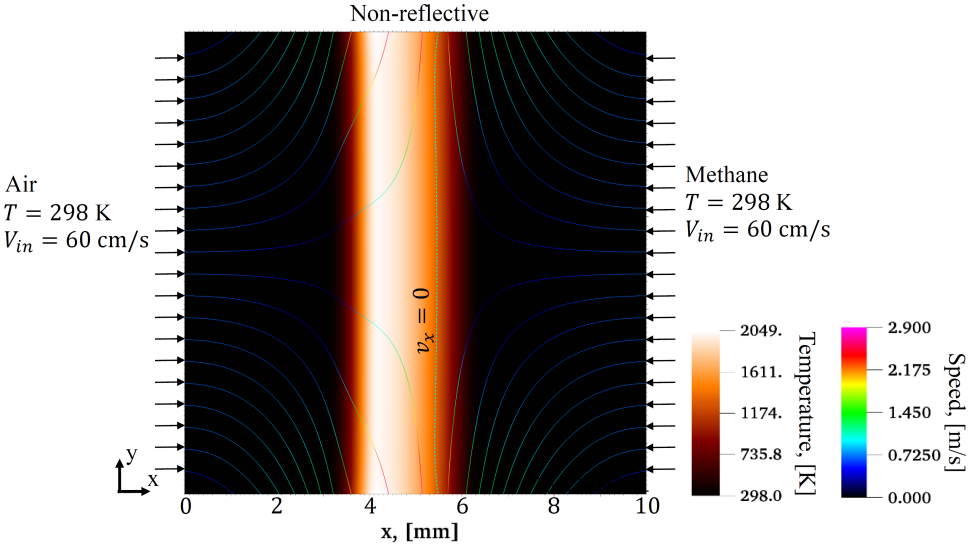

Figure 5. Temperature contour of a 2D counter-flow diffusion flame for methane-air, computed with BIC-FCT-CDM. Also shown are the boundary conditions, domain size, and streamlines. An inflow is imposed on the left with air and on the right with methane. The streamlines are colored by contours of the velocity magnitude. The stagnation plane for the x component of velocity v_x is shown by the dashed blue line.

After demonstrating that the CDM approach can be used to compute a coflow diffusion flame, we investigate whether the structure of a counter-flow diffusion flame. To do this, we consider a two-dimensional square domain with sides that are 10 mm in length, with an inflow of air from the left and an inflow of methane from the right. Here, we choose methane (not n-Heptane) as the fuel so that in future work, we may more easily compare against published results. The boundary conditions and domain are shown in Fig. 5. The speeds of air and methane V_{in} are set equal to each other to balance the momentum (both species are assumed to have the same molecular weight), which ensures a nearly centered stagnation plane. The upper and lower non-reflective boundary conditions extrapolate the first spatial derivative of the primitive variables that is orthogonal to the boundary, so that their second derivative is zero. This is expressed as $d^2b/dy^2 = 0$, where b is a primitive variable. The boundary pressure is extrapolated using a far-field gradient so that a mean pressure is maintained in the interior flow without imposing a strong adverse pressure gradient. This far-field gradient is defined as

$$\left.\frac{dP}{dy}\right|_{boundary} = \frac{P_{boundary} - P_\infty}{L}, \tag{20}$$

where $P_{boundary}$ is the pressure of the interior computational cell closest to the boundary, and P_∞ is the far-field pressure, which we set to be 1 atm. The distance between the boundary and location of the far-field pressure is L, defined to be 100 mm. The domain is discretized using a uniform, Cartesian mesh with $\Delta x = 10/512$ mm.

Figure 5 also shows the contour of temperature with the streamlines, which are colored according to the velocity magnitude. The stagnation plane for $v_x = 0$ is shown as the vertical dashed blue line. Figure 6 shows the quantities of interested from the stagnation streamline of Fig. 5, centered along the y-axis. These are the temperature normalized by its maximum value as the red line, the velocity normalized by V_{in} as the black line, the fuel mass fraction as the blue line, and the air mass fraction as the green line.

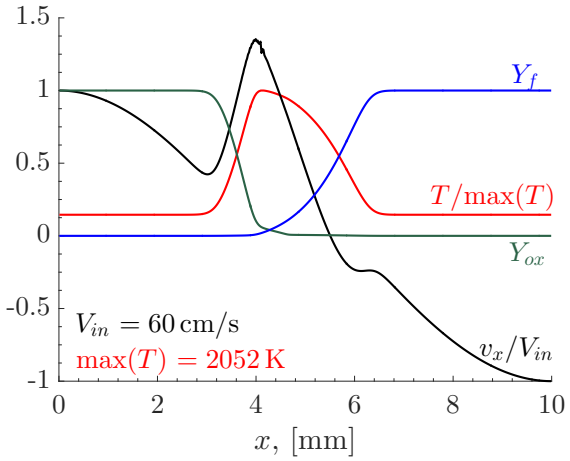

Figure 6. The flow structure along the stagnation streamline of the counter-flow simulation shown in Fig. 5. The blue line is the fuel mass fraction, the green line is the air mass fraction, red is the temperature normalized by the maximum temperature, and black is normalized by the inflow velocity.

There are two important results from this test: (1) The peak temperature and stoichiometric mixture fraction occur on the oxidizer side of the $v_x = 0$ stagnation plane, and (2) the peak temperature is 80 K lower than the maximum value of $T_b(\phi)$ due to the strain effect. This effect is also seen in Fig. 6, which shows that the fuel and oxidizer have failed to completely burn at the location of peak temperature.

Further computations were carried out by varying the inflow velocities V_{in} from 20 to 120 cm/s. These preliminary results show decreasing temperature for increasing strain and flame extinction occurring at $V_{in} = 120$ cm/s. This suggests the CDM approach is capable of computing the effect of strain and extinction, two critical properties of non-premixed flames. Future work will perform further calibration on the diffusive parameters and then compare the results against more detailed chemistry and experimental data in the literature.

V. Conclusions

This work has applied the CDM approach to the simulation of non-premixed diffusion flames. This was done by first simplifying the calibration procedure, which now considers only premixed flames and forgoes the traditional detonation properties. The new calibration matches three target properties: the laminar flame speed S_L, flame thickness Δx_L, and the adiabatic flame temperature T_b. The target parameters were obtained from chemical equilibrium software using the GRI-Mech 3.0 mechanism for methane and a 188-species skeletal mechanism for n-Heptane. The heat release q is calibrated to match T_b. The Arrhenius reaction rate parameters, pre-exponential A and activation energy E_a, are calibrated to match S_L and Δx_L. This process is repeated over a range of equivalence ratios, generating a tabulated list for q, E_a, and A, which is indexed by equivalence ratio.

The CDM was then incorporated into an algorithm which solves the Navier-Stokes equations. The BIC pressure correction was applied to the momentum and energy equations, removing the acoustic limit on the CFL time-step constraint and allowing for efficient computation of low-Mach-number flows. This combined BIC and CDM algorithm was applied to a series of test problems, each testing different aspects of low-Mach-number flames. First, premixed laminar flames were computed and compared against the target properties from the detailed chemistry. The flame properties showed strong agreement. Second, a coflow laminar diffusion flame was computed. The results showed the fuel and oxidizer being depleted at the flame sheet, and the maximum temperature not exceeding the adiabatic flame temperature. These are indications that the balance of heat release, heat conduction, species diffusion, and reaction rate are captured qualitatively well by the CDM. Lastly, we showed that the CDM approach can also compute the structure of a counter-flow diffusion flame. The simulation result showed an 80 K lower peak temperature than the adiabatic flame temperature, the flame-sheet located on the oxidizer side of the stagnation plane, and incomplete burning of reactants at the flame sheet. Future work will extend the calibration procedure to include the diffusion coefficients and compare against detailed chemistry results for counter-flow diffusion flames.

Acknowledgments

This work was supported by the Army Research Office (grant W911NF1710524) and by the National Science Foundation under award CBET 1839510. This work was also supported in part by the University of Maryland through Minta Martin Endowment Funds in the Department of Aerospace Engineering, the Glenn L. Martin Institute Chaired Professorship, and the A. James Clark Distinguished Professorship at the A. James Clark School of Engineering. Computations were performed using the University of Maryland Deepthought2 HPC cluster. The authors also acknowledge the efforts of Dr. Ryan Houim, University of Florida, for his advice and assistance in the implementation of the algorithms.

References

[1]Westbrook, C. K. and Dryer, F. L., "Simplified Reaction Mechanisms for the Oxidation of Hydrocarbon Fuels in Flames," *Combustion Science and Technology*, Vol. 27, No. 1-2, 1981, pp. 31–43.

[2]Fernández-Tarrazo, E., Sánchez, A. L., Linan, A., and Williams, F. A., "A Simple One-Step Chemistry Model for Partially Premixed Hydrocarbon Combustion," *Combustion and Flame*, Vol. 147, No. 1, 2006, pp. 32–38.

[3]Oran, E. S., Boris, J. P., Young Jr, T., Flanigan, M., and Burks, T., "Simulations of Gas Phase Detonations: Introduction of an Induction Parameter Model." Tech. rep., Naval Research Lab Washington D.C., 1980.

[4]Khokhlov, A. M. and Oran, E. S., "Numerical Simulation of Detonation Initiation in a Flame Brush: the Role of Hot Spots," *Combustion and Flame*, Vol. 119, No. 4, 1999, pp. 400–416.

[5]Khokhlov, A. M., Oran, E. S., Chtchelkanova, A. Y., and Wheeler, J. C., "Interaction of a Shock with a Sinusoidally Perturbed Flame," *Combustion and Flame*, Vol. 117, No. 1-2, 1999, pp. 99–116.

[6]Gamezo, V. N., Desbordes, D., and Oran, E. S., "Formation and Evolution of Two-Dimensional Cellular Detonations," *Combustion and Flame*, Vol. 116, No. 1-2, 1999, pp. 154–165.

[7]Kessler, D. A., Gamezo, V. N., and Oran, E. S., "Simulations of Flame Acceleration and Deflagration-to-Detonation Transitions in Methane-Air systems," *Combustion and Flame*, Vol. 157, No. 11, 2010, pp. 2063–2077.

[8]Kessler, D. A., Gamezo, V. N., and Oran, E. S., "Gas-Phase Detonation Propagation in Mixture Composition Gradients," *Phil. Trans. R. Soc. A*, Vol. 370, No. 1960, 2012, pp. 567–596.

[9]Kaplan, C. R., Ozgen, A., and Oran, E. S., "Chemical-Diffusive Models for Flame Acceleration and Transition to Detonation: Genetic Algorithm and Optimization Procedure," *accepted to Combustion Theory and Modeling*, 2018.

[10]Gamezo, V. N., Khokhlov, A. M., and Oran, E. S., "The Influence of Shock Bifurcations on Shock-Flame Interactions and DDT," *Combustion and Flame*, Vol. 126, No. 4, 2001, pp. 1810–1826.

[11]Goodwin, D. G., Moffat, H. K., and Speth, R. L., "Cantera: An Object-oriented Software Toolkit for Chemical Kinetics, Thermodynamics, and Transport Processes," `http://www.cantera.org`, 2017, Version 2.3.0.

[12]Lu, T. and Law, C. K., "Linear Time Reduction of Large Kinetic Mechanisms with Directed Relation Graph: n-Heptane and Iso-Octane," *Combustion and Flame*, Vol. 144, No. 1-2, 2006, pp. 24–36.

[13]Smith, G. P., "GRI-Mech 3.0," *http://www. me. berkley. edu/gri_mech/*, 1999.

[14]Patnaik, G., Guirguis, R. H., Boris, J. P., and Oran, E. S., "A Barely Implicit Correction for Flux-Corrected Transport," *Journal of Computational Physics*, Vol. 71, No. 1, 1987, pp. 1–20.

[15]Zhang, X., Chung, J. D., Kaplan, C. R., and Oran, E. S., "The Barely Implicit Correction Algorithm for Low-Mach-Number Flows," *Computers & Fluids*, Vol. 175, 2018, pp. 230–245.

[16]Boris, J. P. and Book, D. L., "Flux-Corrected Transport. I. SHASTA, a Fluid Transport Algorithm that Works," *Journal of Computational Physics*, Vol. 11, No. 1, 1973, pp. 38–69.

[17]Zalesak, S. T., "Fully multidimensional flux-corrected transport algorithms for fluids," *Journal of computational physics*, Vol. 31, No. 3, 1979, pp. 335–362.

[18]DeVore, C. R., "An Improved Limiter for Multidimensional Flux-Corrected Transport," Tech. rep., Naval Research Lab Washington D.C., 1998.

[19]"Boxlib Users's Guide Website," `https://ccse.lbl.gov/BoxLib/`.